An autopsy case report: Differences in radiological images correlate with histology in Erdheim-Chester disease

Yuuki Ohara,[1] Seiichi Kato,[2] Daisuke Yamashita,[2,3] Akira Satou,[4] Yoshie Shimoyama,[5] Chie Hamaie,[6] Motoki Sato,[7] Nobutaro Ban,[8] Koji Yamamoto,[9] Takehiro Yamada,[10] Hisashi Kawai,[10] Koichi Ohshima,[11] Shigeo Nakamura,[2] and Shinya Toyokuni[1]

[1]Department of Pathology and Biological Responses, Nagoya University Graduate School of Medicine, Nagoya, Japan.
[2]Department of Pathology and Laboratory Medicine, Nagoya University Hospital, Nagoya, Japan.
[3]Department of Pathology, Kobe City Hospital Organization, Kobe City Medical Center General Hospital, Kobe, Japan.
[4]Department of Surgical Pathology, Aichi Medical University Hospital, Nagakute, Japan
[5]Department of Pathology, Nagoya University Hospital, Nagoya, Japan
[6]Department of General Medicine/Family and Community Medicine, Nagoya University Graduate School of Medicine, Nagoya, Japan.
[7]Department of General Medicine, Nagoya University Hospital, Nagoya, Japan.
[8]Medical Education Center, Aichi Medical University School of Medicine, Nagakute, Japan.
[9]Department of Transfusion Medicine, Nagoya University Hospital, Nagoya, Japan.
[10]Department of Radiology, Nagoya University Graduate School of Medicine, Nagoya, Japan.
[11]Department of Pathology, Kurume University School of Medicine, Kurume,

Japan.

Running title: Radio-histological correlation in ECD

All correspondence to: Yuuki Ohara, M.D.
Department of Pathology and Biological Responses, Nagoya University Graduate School of Medicine, 65 Tsurumai-cho, Showa-ku, Nagoya 466-8550, Japan; Tel: +81-52-744-2087; Fax: +81-52-744-2091; E-mail: yuuki.oohara.1196@gmail.com

Conflict of interest: None declared.

Authorship statement

Yuuki Ohara wrote the initial draft of the manuscript and designed the study. All authors have contributed to the data acquisition and critical revision of the manuscript for important intellectual content. All authors approved the final version of the manuscript.

Abstract

p16 activation caused by oncogenic mutations may represent oncogene-induced senescence (OIS), a protective mechanism against oncogenic events. However, OIS can contribute to tumor development via tissue remodeling in some tumors. Erdheim-Chester disease (ECD), a rare non-Langerhans cell histiocytosis, is one such tumor. Its clinical and histological features vary, making it difficult to diagnose. Herein, we describe an autopsy of an ECD patient. The patient underwent radiological examinations, including ^{18}F-fluorodeoxyglucose (FDG)-positron emission tomography/computed tomography (PET/CT), bone scintigraphy and CT. A biopsy from the lesion with the highest FDG accumulation confirmed the presence of foamy macrophages, a diagnostic clue for ECD. Based on this finding and the clinical features, ECD was diagnosed. However, the patient died from heart dysfunction. After the autopsy, each radiologically different site showed various histological findings regarding the morphology of macrophages, fibrosis, inflammation, and p16 expression. OIS-induced histological progression can cause certain changes observed in radiological images. In addition, in order to evaluate the increase in glucose metabolism, which can affect FDG accumulation, the expression of glucose transporter 1 and hexokinase II was also analyzed. Summarizing the radio-histological correlation can help further both the understanding and diagnosis of ECD.

191 words

Key words: Erdheim-Chester disease, oncogene-induced senescence, radio-histological correlation, ^{18}F-fluorodeoxyglucose-positron emission tomography/computed tomography, bone scintigraphy, hexokinase II, autopsy, non-Langerhans cell histiocytosis

Introduction

Erdheim-Chester disease (ECD) is a type of non-Langerhans cell histiocytosis (LCH) and is thought to arise from the monocyte-macrophage lineage. Although several hundred cases of ECD have been reported internationally,[1-3] there is no report that describes in detail the correlations between radiological images and histological findings. ECD involves multiple organs (*e.g.*, bone/retroperitoneum/heart/vessels/lungs/central nervous system/skin/orbits).[1-3] Non-Langerhans macrophages, foamy macrophages and multinucleated giant cells, which are positive for CD68 and CD163 but negative for CD1a and S-100, together with fibrosis and non-neoplastic inflammatory cells, infiltrate these sites.[1] These findings are classical features of ECD. However, it seems that foamy macrophages do not always invade the entire body, and varying histological features are present.[1] Although *BRAFV600E*, *NRAS* or *PIK3CA* gene mutations have been reported,[4] these mutations are currently not necessary for diagnosis.[1,2] Rather, clinical features and histological findings have been emphasized in making a diagnosis. Networks of cytokines and chemokines exist in ECD,[5] and interferon (IFN)-α can be the first-line therapy.[1,2]

Some oncogenes (*BRAF*, *RAS*) activate tumor suppressor genes, such as the *p16* and RB families, which induce cell senescence to prevent oncogenic events. This mechanism is called oncogene-induced senescence (OIS) and is known to occur in some tumors including ECD.[6-8] Conversely, the senescent cells produce a senescence-associated secretory phenotype (SASP), including cytokines and growth factors. The SASP causes infiltration of wild-type inflammatory cells and tissue remodeling and paradoxically promotes oncogenesis.[9,10]

Herein, we report an autopsy case of an ECD patient with few foamy macrophages. The clinical and histological features are precisely described with

100 pathophysiological considerations.

101

Clinical summary

A 74-year-old previously healthy male was found to have leukopenia (white blood cells, WBCs, 2,500/μl) and thrombocytopenia (platelets, 85,000/μl) at a health evaluation 10 years prior to his death and was followed up at our hospital. He experienced repeated low-grade fevers of 37°C of unknown etiology during the last year before his death. Seven months before his death, he had repeated episodes of high fevers of 38°C, and a disturbance of ocular mobility was noticed. Thoracic to abdominal computed tomography (CT) revealed a soft tissue-like silhouette surrounding the aorta (**Fig. 1A**) and kidney (**Fig. 1B**).[11] Malignant lymphoma, aortitis syndrome, amyloidosis and IgG4-related disease were suspected, and a posterior ilium biopsy and inguinal lymph node biopsy were performed. However, only hypercellular bone marrow and lymphadenitis, respectively, were observed. In the last month prior to his death, a CT scan indicated the appearance of a soft tissue-like silhouette surrounding the heart and mesentery and an increase in pleural/pericardial effusions. The patient was therefore admitted to our hospital for further examination. During the year of his death, he lost 10 kg in body weight (from 65 to 55 kg).

The laboratory data at the time of his hospitalization revealed the following: WBC count, 5,300/μl (neutrophils, 42.8%; lymphocytes, 22.3%; monocytes, 42.0%); hemoglobin, 12.7 g/dl; platelets, 87,000/μl; CRP, 3.60 mg/dl; and ESR, 27 mm/h. A physical examination and magnetic resonance imaging (MRI) revealed tumors in both orbits (**Fig. 1C**).[11] Whole-body ^{18}F-fluorodeoxyglucose (FDG)-positron emission tomography/computed tomography (PET/CT) revealed remarkably high (the highest) accumulation of FDG in the right ilium (**Fig. 1D**).[11] The maximum standardized uptake value (SUVmax) of the site was 12.87. A slight to moderate increase of FDG accumulation was also observed in the other

parts of the body (**Fig. 1E**). However, it was difficult to determine whether these slight to moderate increases show tumor itself or reactive change of bone marrow. Reactive change in FDG-PET/CT can be encountered in various clinical conditions such as chronic inflammation (*e.g.*, rheumatoid arthritis, sarcoidosis), tumor and anemia. Symmetrically increased osteoblastic activity primarily in the tibias and the second lumbar vertebra was detected on ^{99m}technetium hydroxymethylene diphosphonate (^{99m}Tc-HMDP) bone scintigraphy (**Fig. 1F**). Based on these findings, malignant lymphoma, IgG4-related disease and ECD were suspected, and a biopsy of the right ilium was performed in the area where FDG maximally accumulated (**Fig. 1D**). The biopsy showed macrophages, multinucleated giant cells, foamy macrophages, lymphocytic infiltrate and fibrosis (see pathological findings for further details). Almost all the macrophages were positive for CD68/CD163 but negative for CD1a/S-100/Langerin. No evidence of emperipolesis was present. Fungal infection and tuberculosis were excluded by PAS and Ziehl-Neelsen staining. Based on these findings, the patient was diagnosed with ECD, and IFN-α was administered. The patient received subcutaneous injections of 6,000,000 units/time of IFN-α (3 times per week) for approximately one week. However, the increase in the pleural and pericardial effusions was so difficult to control that the patient developed atrial fibrillation and died from heart dysfunction and respiratory failure despite pericardial drainage.

Pathological findings

The autopsy was performed one and a half hours after death. The patient's body height was 166 cm, and his weight was 60.4 kg. Pretibial edema was observed. Macroscopically, the tumor was elastic hard/yellowish with accompanying fibrosis and had grown predominantly in fat-rich tissues including the pleura (**Fig. 2A**), pericardium/periaortic tissue (**Fig. 2B**), retroperitoneum/renal capsule (**Fig. 2C**), and mesentery (**Fig. 2D**). A part of the second lumbar vertebra, which corresponded to the accumulation of ^{99m}Tc-HMDP (**Fig. 1E**), was replaced by fibrosis (**Fig. 2E**). Histologically, a number of monocytes/macrophages were observed in the multiple organs (*e.g.*, bone marrow of the entire vertebrae/spleen/thyroid gland/lung/pleura/aorta/heart/pericardium/kidney/retroperitoneum/renal capsule/suprarenal gland/pancreas/mesentery/peritoneum/testis. Macrophages were dominantly observed around fat-rich tissues, such as the pleura, pericardium and mesentery, rather than the stroma, vessels and parenchyma of organs. We speculated that the patient had died from diastolic dysfunction of the heart caused by the tumor itself and fibrosis around the pericardium.

Notably, foamy macrophages were observed only in the right ilium, where FDG maximally accumulated. In addition, each radiologically different site showed various histological features of macrophages, inflammation, fibrosis, and p16 expression. We analyzed the radio-histological correlation as follows: #1. Sites without radiological characteristics (hematopoietic organs such as spleen and bone marrow of vertebrae), #2. A scintigraphy-positive site (second lumbar vertebra), #3. The highest FDG site (right ilium), and #4. CT low sites (fat-rich membranes, including the pleura, pericardium and mesentery) (**Fig. 3**). At site #1, monocytes had proliferated without fibrosis. Silver impregnation and Masson

trichrome staining showed that a small amount of reticular fibers had proliferated. This finding corresponds to MF-0 in the European consensus on grading of bone marrow fibrosis.[12] At site #2, multinucleated macrophages, spindle-shaped macrophages, inflammatory cells and reticular/collagen fibers (MF-2~3) were observed (defined as #2a). A greater amount of fibrosis was observed in the area with spindle-shaped macrophages in #2a. Much greater fibrosis (MF-3), few macrophages and inflammatory cells were partially observed (defined as #2b). At site #3, foamy macrophages and a greater number of inflammatory cells appeared. The fibrosis was composed of diffuse reticular fibers (MF-2). At site #4, invasion of macrophages and multinucleated cells with collagen fiber fibrosis and inflammation were observed. Connective tissue growth factor (CTGF),[13] a fibrosis marker, was weakly to moderately positive (Table 1). The percentage of p16-positive macrophages was calculated at each site (**Table 1**). The monocytes/macrophages did not express cyclin D1, p21 and p53 at any of the sites. The Ki-67 proliferative index was 5-10% at all the sites.

FDG-PET/CT illustrates the increase in glucose metabolism in a lesion (*e.g.*, inflammation or tumor). This metabolic increase is caused by various factors including the expression of glucose transporter (Glut) and hexokinase (HK), and mitochondrial activity.[14, 15] To clarify the reasons why extremely high FDG accumulated at site #3, we analyzed the expression of glucose transporter 1 (Glut-1) and hexokinase II (HK-II). Glut-1 was negative at all sites, whereas HK-II was strongly positive at site #3 compared to the other sites (**Fig. 4A**).

BRAFV600, *NRAS* and *PIK3CA* mutations were examined from DNA samples of paraffin sections. *BRAFV600* and *PIK3CA* mutations were examined by direct sequencing, and *NRAS* mutations were examined by polymerase chain reaction-reverse sequence specific oligonucleotide method (SRL, Inc., Tokyo,

Japan). These mutations were not detected. Immunohistochemically, we examined BRAF mutations using an anti-BRAFV600E antibody in the right ilium, bone marrow, lung and heart. All sites were negative for this mutation based on immunohistochemical examination.

Discussion

Although it is emphasized that foamy macrophages proliferate in ECD, foamy macrophages may not always invade the entire body.[1] The foamy macrophage is considered to indicate a diagnosis of ECD. Thus, if the biopsy shows only the proliferation of non-foamy macrophages, it is difficult to exclude other diseases, including inflammation and other histiocytic tumors. In this context, summarizing radio-histology can be a practical method for determining where to perform a biopsy.

In general, FDG-PET can portray the increase in glucose metabolism as the result of high turnover/proliferation in the lesion, and bone scintigraphy can show reactive changes (*e.g.*, osteogenesis/remodeling/fibrosis) of the bone near the lesion. The CT absorption value reflects the characteristics of a substance. Although these images cannot simply be compared to each other, we can possibly infer the activity/histology of the lesion by integrating such information in ECD.

This case indicates that histology (tissue remodeling) of ECD is associated with OIS (**Fig. 4B**). This is supported by the positive correlation between macrophage expression of p16 and the increase in inflammatory cells infiltrating the lesion (**Fig. 3 and Table 1**). The changes in histology or senescent conditions can affect radiological images. We described the area with the highest FDG accumulation as site #3, where foamy macrophages expressed higher levels of HK-II. Foamy macrophages may proliferate faster than the macrophages at other sites and site #3 may be more aggressive. More than a certain value of SUVmax might indicate the presence of foamy macrophages. High expression of p16 was also observed at site #3. This fact supports that site #3 was more aggressive, considering the fact that p16 expression positively correlates with the grade of cervical intraepithelial neoplasia (CIN).[16] In contrast, the number of tumor cells

decreased and p16 expression was not observed at site #2b. Senescence control might successfully suppress tumor growth. Thus, we believe that site #2b is in the last stage of ECD. Greater fibrosis (#2) was observed where ^{99m}Tc-HMDP accumulated, and bone scintigraphy is thought to show remodeled tissue. Based on these facts, FDG-PET/CT may be more convenient to determine where a biopsy should be performed. In this case, no expression of p21, p53, and proteins of another senescent pathway[6,10] was observed. This is compatible with a study that found that p53 degradation induces p16 expression and SASPs.[17]

The examination performed to detect mutations in this report has some limitations. Non-neoplastic macrophages may be used for sequencing, which resulted in an absence of mutations. Moreover, although no mutations were found in our case, overexpression of p16 was surely ascertained. This fact may indicate that an unknown mutation is present other than those previously identified. Cases of LCH without the BRAFV600E mutation and with p16 expression have been reported and the same reason was proposed.[18]

In conclusion, investigating the tissue remodeling that corresponds to radiological images can help understanding the pathophysiology of ECD as well as improving our ability to diagnose and treat ECD.

1,998 words

Acknowledgments

We thank Mr. Nobuaki Misawa (Nagoya University Graduate School of Medicine) for technical assistance. Yuuki Ohara was a recipient of Takeda Science Foundation Fellowship (April 2014-March 2018).

Disclosure statement

None Declared.

References

1 Diamond EL, Dagna L, Hyman DM*, et al.* Consensus guidelines for the diagnosis and clinical management of Erdheim-Chester disease. *Blood*. 2014; **124**: 483-92.

2 Mazor RD, Manevich-Mazor M, Shoenfeld Y. Erdheim-Chester Disease: a comprehensive review of the literature. *Orphanet J Rare Dis*. 2013; **8**: 137.

3 Veyssier-Belot C, Cacoub P, Caparros-Lefebvre D*, et al.* Erdheim-Chester disease. Clinical and radiologic characteristics of 59 cases. *Medicine (Baltimore)*. 1996; **75**: 157-69.

4 Emile JF, Diamond EL, Helias-Rodzewicz Z*, et al.* Recurrent RAS and PIK3CA mutations in Erdheim-Chester disease. *Blood*. 2014; **124**: 3016-9.

5 Stoppacciaro A, Ferrarini M, Salmaggi C*, et al.* Immunohistochemical evidence of a cytokine and chemokine network in three patients with Erdheim-Chester disease: implications for pathogenesis. *Arthritis Rheum*. 2006; **54**: 4018-22.

6 Mooi WJ, Peeper DS. Oncogene-induced cell senescence--halting on the road to cancer. *N Engl J Med*. 2006; **355**: 1037-46.

7 Cangi MG, Biavasco R, Cavalli G*, et al.* BRAFV600E-mutation is invariably present and associated to oncogene-induced senescence in Erdheim-Chester disease. *Ann Rheum Dis*. 2014.

8 Cavalli G, Biavasco R, Borgiani B, Dagna L. Oncogene-induced senescence as a new mechanism of disease: the paradigm of erdheim-chester disease. *Front Immunol*. 2014; **5**: 281.

9 Coppe JP, Desprez PY, Krtolica A, Campisi J. The senescence-associated secretory phenotype: the dark side of tumor suppression. *Annu Rev Pathol*. 2010; **5**: 99-118.

10 Di Mitri D, Alimonti A. Non-Cell-Autonomous Regulation of Cellular Senescence in Cancer. *Trends Cell Biol*. 2016; **26**: 215-26.

11 Takehiro Yamada HK, Yusuke Sakurai, et al. A case of histiocytosis struggled to diagnosis. *Eizojoho Medical*. 2015; **47**: 620-21.

12 Thiele J, Kvasnicka HM, Facchetti F, Franco V, van der Walt J, Orazi A. European

287 consensus on grading bone marrow fibrosis and assessment of cellularity. *Haematologica*.
288 2005; **90**: 1128-32.
289 13 Wells JE, Howlett M, Cole CH, Kees UR. Deregulated expression of connective tissue
290 growth factor (CTGF/CCN2) is linked to poor outcome in human cancer. *Int J Cancer*. 2015;
291 **137**: 504-11.
292 14 Zhao S, Kuge Y, Mochizuki T*, et al.* Biologic correlates of intratumoral heterogeneity in
293 18F-FDG distribution with regional expression of glucose transporters and hexokinase-II in
294 experimental tumor. *J Nucl Med*. 2005; **46**: 675-82.
295 15 Aloj L, Caraco C, Jagoda E, Eckelman WC, Neumann RD. Glut-1 and hexokinase
296 expression: relationship with 2-fluoro-2-deoxy-D-glucose uptake in A431 and T47D cells in
297 culture. *Cancer Res*. 1999; **59**: 4709-14.
298 16 Branca M, Ciotti M, Santini D*, et al.* p16(INK4A) expression is related to grade of cin and
299 high-risk human papillomavirus but does not predict virus clearance after conization or
300 disease outcome. *Int J Gynecol Pathol*. 2004; **23**: 354-65.
301 17 Johmura Y, Sun J, Kitagawa K*, et al.* SCF(Fbxo22)-KDM4A targets methylated p53 for
302 degradation and regulates senescence. *Nat Commun*. 2016; **7**: 10574.
303 18 Chilosi M, Facchetti F, Calio A*, et al.* Oncogene-induced senescence distinguishes indolent
304 from aggressive forms of pulmonary and non-pulmonary Langerhans cell histiocytosis. *Leuk*
305 *Lymphoma*. 2014; **55**: 2620-6.
306 19 Laberge RM, Sun Y, Orjalo AV*, et al.* MTOR regulates the pro-tumorigenic senescence-
307 associated secretory phenotype by promoting IL1A translation. *Nat Cell Biol*. 2015; **17**: 1049-
308 61.
309 20 Gianfreda D, Nicastro M, Galetti M*, et al.* Sirolimus plus prednisone for Erdheim-
310 Chester disease: an open-label trial. *Blood*. 2015; **126**: 1163-71.
311

Tables

Table 1. Summary of histological findings. The histological findings in **Fig. 3** are summarized. Higher macrophage expression of p16 indicates greater inflammatory cell infiltration into the lesion. Infiltration of inflammatory cells is described as follows: -, < 20/high-power field; +, 20-100/high-power field; ++, > 100/high-power field. CTGF, connective tissue growth factor; ±, weakly positive; +, moderately positive.

Radiological images		Monocyte/macrophage type	Fibrosis	Infiltration of inflammatory cells	p16 (%)	CTGF
#1. Without characteristics		Proliferation of monocytes	Reticular fiber±, MF-0	-	0	+
#2. Scintigraphy positive	#2a	Multinucleated macrophages Spindle macrophages	Reticular fiber+, MF-2~3	+	21.6	+
	#2b	Decrease in cells	Collagen fiber+++, MF-3	-	0	±
#3. The highest FDG		Multinucleated and foamy macrophages	Reticular fiber+, MF-2	++	48.7	±
#4. CT low		Multinucleated macrophages	Collagen fiber+	+	18.4	+

Figures

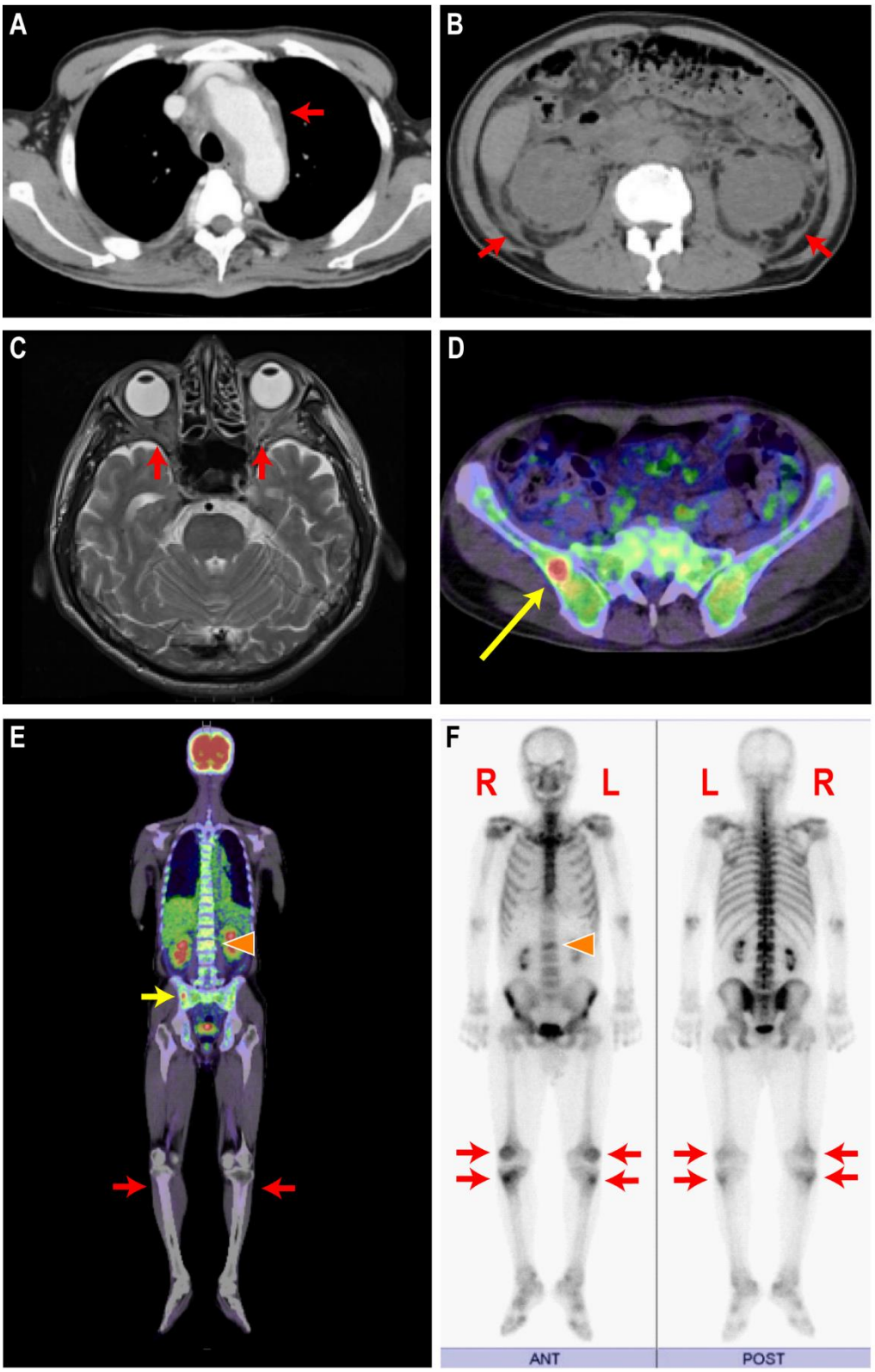

Figure 1. Radiological findings. (A, B) Soft tissue-like silhouette (arrows)

surrounding the aorta (A) and kidney (B) on CT images. The perirenal silhouette is known as "hairy kidney" appearance. (C) Tumors (arrows) in both orbits on MRI (T2-weighted image). (D) An accumulation of FDG (SUVmax, 12.87) in the right ilium on FDG-PET/CT. SUVmax of the other parts of the ilium was 3.82. (E) A slight to moderate increase of FDG uptake also observed in the other parts of the body. SUVmax was as follows: Second lumbar vertebra (arrow heads), 7.05; the other vertebras, 3.57-5.02; mesentery, 2.81-3.07; left tibias, 1.87; right tibias, 1.63. The red color arrows indicate tibias. The yellow color arrow indicates the same lesion described in (D). (F) Symmetrically increased osteoblastic activity primarily in the tibias/patellas (arrows) and the second lumbar vertebra (arrows heads) detected on bone scintigraphy. L, left; R, right.

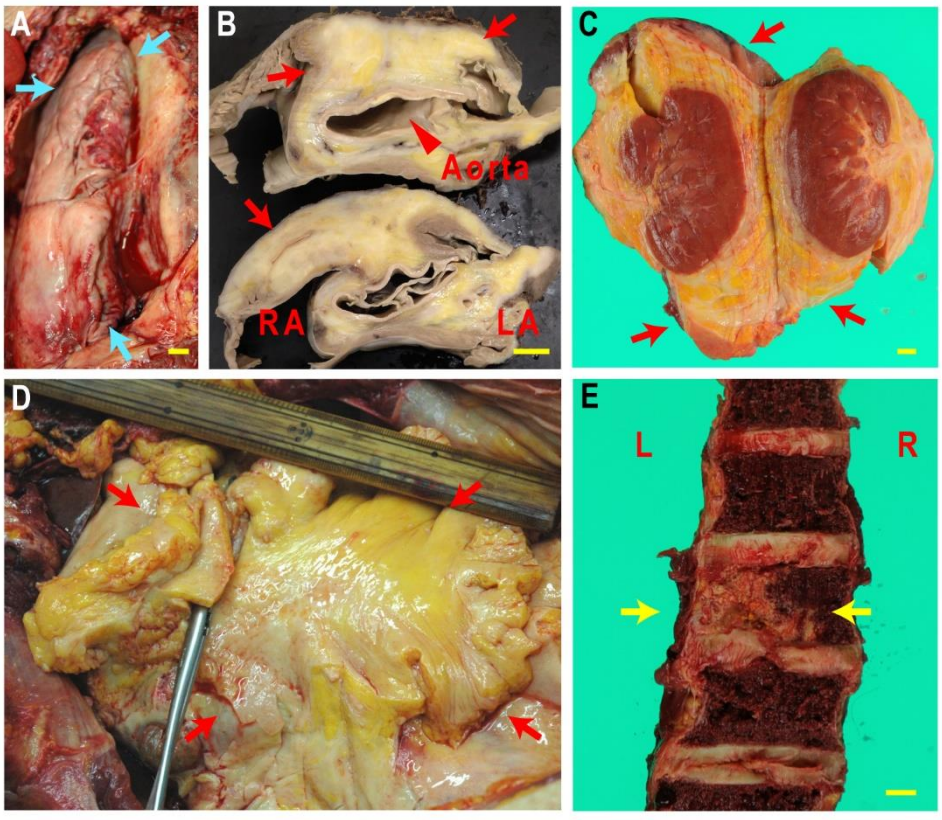

Figure 2. Macroscopic findings of the extensive tumor. An elastic hard and

yellowish tumor accompanied by fibrosis was growing in the pleural and peritoneal cavities. (A-C) The lung (A), aorta and heart (B), and renal capsule (C) were surrounded by the tumor (arrows). (D) The mesentery (arrows) was yellowish and thick. (E) The second lumbar vertebra was partially accompanied by strong fibrosis (arrows), which corresponded to the increased osteoblastic activity detected on bone scintigraphy. Scale bar, 10 mm. LA, left atrium; RA, right atrium; L, left; R, right

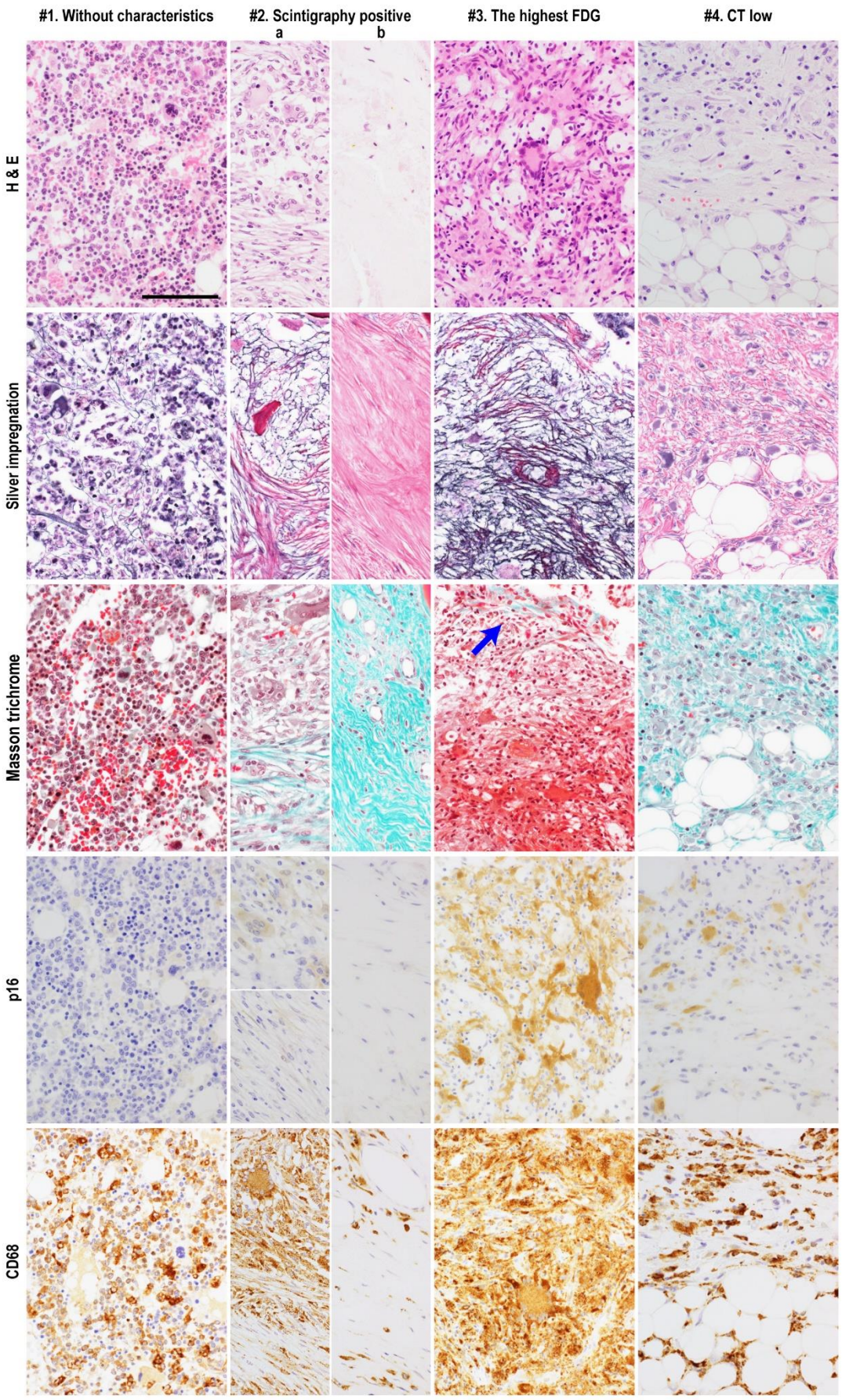
#1. Without characteristics
#2. Scintigraphy positive
a
b
#3. The highest FDG
#4. CT low
H & E
Silver impregnation
Masson trichrome
p16
CD68

348

Figure 3. Radiological images correlated with tissue remodeling in histological findings. (#1) Sites without radiological characteristics. Proliferation of monocytes without fibrosis was observed. Silver impregnation and Masson trichrome staining revealed proliferation of a small amount of reticular fibers (MF-0). (#2) Scintigraphy-positive site. Multinucleated macrophages, spindle-shaped macrophages, inflammatory cells and reticular/collagen fibers (MF-2~3) were observed (defined as #2a). Greater fibrosis (MF-3), fewer macrophages and inflammatory cells were partially observed (defined as #2b). (#3) The highest FDG site. Foamy macrophages and a greater number of inflammatory cells were present. The fibrosis was composed of diffuse reticular fibers (MF-2) and focal collagen fibers (arrow). (#4) CT low site. Invasion of macrophages and multinucleated cells with collagen fiber fibrosis and inflammation were observed. #1, bone marrow of lumbar vertebrae; #2, bone marrow of the second lumbar vertebra; #3, right ilium; #4, mesentery. All figures are at the same magnification, and the scale bar in (#1-HE) is 100 μm.

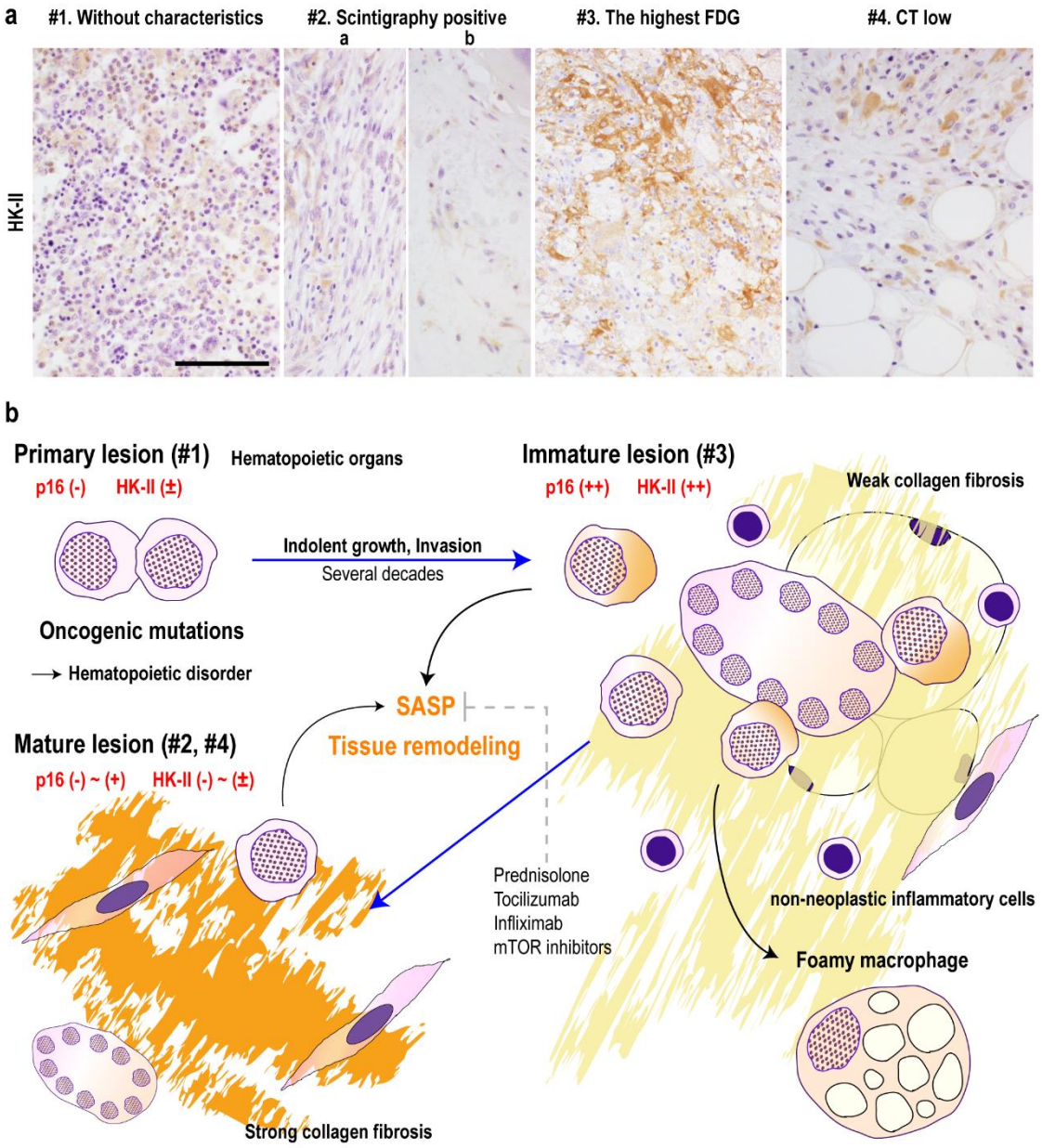

Figure 4. Hexokinase II (HK-II) expression and pathophysiology of ECD. (A) HK-II was strongly positive at site #3, compared to the other sites (#1, weak; #2a, weak; #2b, negative; #3, strong; #4, weak). Stronger HK-II expression at site #3 and lower HK-II expression at site #1, #2 and #4 are consistent with FDG accumulation. All figures are at the same magnification, and the scale bar in (#1) is 100 μm. (B) Oncogenic mutations of monocytes first occur in hematopoietic organs (#1). Invaded macrophages have a unique affinity for fat tissues (#2, #3,

#4). OIS, as detected by p16 expression, is possibly associated with tumor progression and tissue remodeling (fibrosis/non-neoplastic inflammation) through SASPs. Judging from the degree of fibrosis, site #2 and #4 is thought to be in later stage. Fibrosis, rather than tumor itself, can lead to fatal conditions (*e.g.*, diastolic dysfunction of heart), and may represent an important target for managing ECD. Drugs that may inhibit SASPs (*e.g.*, anti-inflammatory drugs,[1] cytokine-blocking agents,[7,8] mTOR inhibitors[19,20]) are available. ECD, Erdheim-Chester disease; mTOR, mammalian target of rapamycin; OIS, oncogene-induced senescence; SASP, senescent associated secretary phenotype.